Constraining mantle carbon: CO_2-trace element systematics in basalts and the roles of magma mixing and degassing

Simon Matthews[a]*, Oliver Shorttle[a,b], John F. Rudge[a], John Maclennan[a]

a. Department of Earth Sciences,
University of Cambridge
Downing Street
Cambridge
CB2 3EQ

b. Institute of Astronomy,
University of Cambridge
Madingley Road
Cambridge
CB3 0HA

*Corresponding author (sm905@cam.ac.uk)

Abstract

Our present understanding of the mantle carbon budget is in part built upon measurements of carbon concentrations in olivine hosted melt inclusions. Only a small number of such datasets are thought to have avoided degassing, having been entrapped prior to CO_2 vapour saturation, and are therefore able to constrain primary CO_2 concentrations. The absence of degassing in melt inclusion datasets has been inferred from the presence of strong correlations between CO_2 and trace elements. In this

contribution, we demonstrate that partial degassing followed by magma mixing not only retains such positive correlations, but can enhance them.

Simple models of magma mixing and degassing are used to characterise how CO_2-trace element systematics respond to CO_2 vapour saturation in primary mantle melts entering the crust, followed by magma mixing. Positive correlations are expected between CO_2 and most trace elements, and the average CO_2/Ba and CO_2/Nb ratios are controlled by the pressure of magma storage, rather than the CO_2 concentration in the mantle. We find that the best estimates of mantle CO_2 are the maximum CO_2/Ba ratios observed in melt inclusion datasets, though a large number of analyses are required to adequately characterise the maximum of the CO_2/Ba distribution. Using the mixing and degassing models we estimate the number of analyses required to obtain a maximum CO_2/Ba observation within 10% of the mantle value.

In light of our results, we reassess existing melt inclusion datasets, and find they exhibit systematics associated with partial degassing and mixing. We argue that all the data presently available is consistent with a depleted mantle CO_2/Ba ratio of ~140, and there is as yet no evidence for heterogeneity in the CO_2/Ba ratio of the depleted mantle.

Key Words: Mantle, Carbon, Ratios, Degassing, Mixing, Inclusions

1 Introduction

The mantle is the largest reservoir by mass in the Earth and through volcanism and subduction remains in continual chemical communication with Earth's atmosphere and oceans. Carbon is a key element in this cycle, providing thermostatic control on Earth's climate via silicate weathering and carbonate subduction (Walker et al., 1981; Hayes and Waldbauer, 2006). Though the concentration of carbon in Earth's mantle is thought to be low (≤300 ppm; Javoy and Pineau, 1991; Saal et al., 2002; Cartigny et al., 2008; Michael and Graham, 2015; Le Voyer et al., 2017), the mantle carbon budget may greatly exceed that in any other reservoir (Cartigny et al., 2008; Hirschmann and Dasgupta, 2009; Dasgupta and Hirschmann, 2010; Dasgupta, 2013; Kelemen and Manning, 2015). In order to understand how the Earth's habitable surface environment was formed and regulated over geological time, the whole-Earth Carbon cycle must be understood (Kasting et al., 1993). The first step in this process is understanding the volatile budgets of major terrestrial reservoirs such as the mantle. Our current understanding is, however, fragmentary due to the scarcity of robust observational constraints on the carbon content of undegassed mantle-derived magmas.

Estimates of the carbon concentration of the depleted mantle are based on a small number of basaltic glass datasets, summarised in Figure 1, and the $CO_2/^3He$ ratio of hydrothermal fluids. Marty (2012) estimate the CO_2 content of the depleted mantle to be 183±92 ppm using a $C/^3He$ ratio of $2.2 \pm 0.6 \times 10^9$ (Resing et al., 2004) and a ^3He mid-ocean ridge flux of 1000±250 mol yr^{-1} (Craig et al., 1975). If the mid ocean ridge ^3He flux is substantially lower, as suggested by Bianchi et al. (2010), the same $CO_2/^3He$ ratio would imply a depleted mantle CO_2 content of ~96 ppm. Primary CO_2 concentrations in basaltic glasses have been inferred by numerous methods: by correcting for degassing using C isotope fractionation (Cartigny et al., 2008); by using Cl concentrations as a proxy for CO_2

concentrations (Shimizu et al., 2016); by using maximum values of CO_2/Nb ratios in partially degassed datasets (Shaw et al., 2010; Helo et al., 2011; Wanless et al., 2014); and by looking at the covariation of CO_2 with Nb or Ba in undegassed suites (Hauri et al., 2002; Saal et al., 2002; Michael and Graham, 2015; Shimizu et al., 2016; Le Voyer et al., 2017). It is this final observational approach that we focus on in this contribution, since undegassed melts provide the most direct constraint on mantle CO_2 concentrations and their CO_2-trace element systematics can additionally provide a probe of the redox state of mantle carbon (Eguchi and Dasgupta, 2017). Basaltic glasses can preserve undegassed CO_2 either by being entrapped as melt inclusions in growing olivines (Hauri et al., 2002; Saal et al., 2002; Le Voyer et al., 2017), or by having sufficiently low CO_2 concentrations that they remain undersaturated following eruption (Michael and Graham, 2015; Shimizu et al., 2016). Mantle CO_2 concentrations inferred from these datasets range from 60-137 ppm. We consider the roles that mixing and degassing may have played in the generation of these glasses, and re-evaluate mantle CO_2 budgets in light of this.

In order to understand the effects of concurrent magma mixing and degassing on melt inclusion compositions, we use a statistical mixing model combined with simple models for mantle melting and CO_2 saturation (Section 2). This mixing-degassing model is used to understand the general behaviour of CO_2–trace element systematics in Section 3. The implications of these models for the CO_2 budget and the presence of CO_2 heterogeneity in the depleted mantle are discussed in Section 4.

1.1 Comparing CO_2 to lithophile trace elements

The presence of correlations between CO_2 and highly incompatible trace elements in suites of co-genetic CO_2-undersaturated glasses (Figure 2), has become an important empirical basis for inferring the behaviour of CO_2 during mantle melting and degassing.

The strong correlation between CO_2 and Nb in such glass datasets underlies the inference of a close correspondence between the behaviour of CO_2 and Nb during mantle melting (Saal et al., 2002). This interpretation has been nuanced by recent experimental results, that show that CO_2 behaves more incompatibly than Nb, having a bulk mantle-melt partition coefficient closer to that of Ba (Rosenthal et al., 2015).

During differentiation and crustal processing, the persistence of correlated enrichments and depletions of incompatible trace elements and CO_2 is thought to imply that CO_2 has remained soluble in the melt. Le Voyer et al. (2017) and Saal et al. (2002) identify their melt inclusion suites as being undegassed on this basis. Rosenthal et al. (2015) instead suggest that many of the samples in such co-genetic suites have lost CO_2, based on their scatter to low CO_2/Nb ratios (Figure 2). Understanding the controls on CO_2-trace element systematics is therefore vital for assessing if mantle CO_2/trace element ratios are reflected in basalts.

1.2 The role of mixing in generating trace element systematics

Near-fractional melting of the mantle is expected to generate melts with diverse trace element chemistry. Although considerable variation in trace element concentrations is found in some melt inclusions suites (e.g. Sobolev et al., 1994), it is still significantly less than the diversity predicted from models of fractional melt generation (Kelemen et al., 1997a; Maclennan et al., 2003). In more evolved basaltic matrix glasses, very little variation is preserved (Maclennan, 2008). This decrease in variability with melt evolution has been understood in terms of concurrent mixing and crystallisation (Sobolev, 1996; Maclennan, 2008; Shorttle et al., 2016). The mixing process can efficiently dilute the most incompatible trace-element enriched, and therefore CO_2

enriched, fractional melts prior to melt inclusion entrapment even in primitive olivine macrocrysts.

Simple statistical models of melt mixing have been able to reproduce many of the observed chemical systematics of melt inclusion and glass suites (Rudge et al., 2013; Shimizu et al., 2016; Shorttle et al., 2016). These models utilise the properties of the Dirichlet distribution to model the geochemical consequences of progressive mixing of mantle melts. We build upon such models here, applying them to the creation of volatile element variability in mantle-derived melts and the destruction of this variability by mixing and degassing in the crust.

2 Modelling concurrent mixing and degassing

The model comprises three sequential processes, summarised in Figure 3. Firstly, a melting model for passively upwelling mantle is used to generate the masses and chemistry of fractional melts for a typical mid-ocean ridge (Section 2.1, Figure 3a). These melts are then placed at a pressure corresponding to magma storage in the crust, and melts that are oversaturated in CO_2 degas until they are in equilibrium (Section 2.2, Figure 3b). Finally, the melts are partially mixed (Section 2.3, Figure 3c). We do not attempt to model fractional crystallisation since the melt inclusions preserving primary CO_2/Nb and CO_2/Ba ratios represent the most primitive melts.

2.1 Melting Model

To generate the fractional melts used by the mixing and degassing model, we first calculate the melt extracted, X, as a function of pressure for passively upwelling mantle using the parameterization of lherzolite melting by Katz et al. (2003). We set the mantle potential temperature to 1318°C, a temperature appropriate for normal mid-ocean ridges (Matthews et al., 2016), and cease melting once the base of the crust is reached. A

pressure, P, decrement of 0.006 GPa is used during numerical integration of the melting equations. For computational convenience we then remap the results of these calculations from $X(P)$ to $P(X)$, in steps of equal melt fraction increment (0.01%) using linear interpolation.

The trace element chemistry of the generated melts is calculated assuming near fractional melting, modelled with the equation:

$$C_l = \frac{C_0}{(1-\Phi)D+\Phi}\,(1-X)^{\frac{(1-\Phi)(1-D)}{(1-\Phi)D+\Phi}},$$

(Zou, 2007 equation 3.7), where C_l and C_0 are the concentrations of the trace element in the liquid and original solid, D is the partition coefficient (for simplicity assumed independent of pressure), Φ is the residual melt fraction, and X is fraction of extracted melt. The concentrations of trace elements initially in the solid are set to those in 'Average DMM' of Workman & Hart (2005). The liquid compositions are calculated assuming Φ = 0.5% by mass and Ds appropriate for typical melting conditions of lherzolite (Workman and Hart, 2005). Initial CO_2 concentrations in the melts are calculated in the same manner, assuming a bulk partition coefficient of 5.5×10^{-4} (Rosenthal et al., 2015) and a CO_2/Ba ratio in the solid of 140, except where noted otherwise.

In these calculations we consider meltgeneration from a single chemically homogenous lithology. Though there is evidence for heterogeneity in the depleted mantle, the contribution of melts from heterogeneous domains is likely small (Hirschmann and Stolper, 1996; Matthews et al., 2016). Furthermore, we find melting of a single homogeneous source reproduces the observed CO_2-trace element systematics adequately. In Appendix C we demonstrate how varying some of the constants used in the melting model affects the statistics described in Section 3.

2.2 Degassing Model

Once mantle melts have been generated, they may be transported upwards through the mantle in high porosity channels, allowing much of the geochemical variability arising from the melting process to be retained (Spiegelman and Kelemen, 2003). At depths where the melt fraction is not sufficient for high porosity melt channels to form, the melts may become homogenised (Rudge et al., 2013), though this process has only a minor effect on the conclusions drawn here (Appendix A).

Melts can only be preserved in melt inclusions once they have begun to crystallise. Structural and geochemical observations from the Oman ophiolite (Boudier et al., 1996; Kelemen et al., 1997b), and magma storage pressures derived from OPAM and clinopyroxene-melt barometry performed on samples from the Icelandic rift zones and mid-ocean ridges (Maclennan et al., 2001; Herzberg, 2004; Winpenny and Maclennan, 2011; Neave and Putirka, 2017), indicate that crystallisation in oceanic rift settings begins beneath the Moho and proceeds to low pressure. This process is shown schematically in Figure 3a.

The pressure of MORB crystallisation will have a major control on how much of mantle-derived CO_2 variability is preserved in melt inclusions, as pressure is the primary control on CO_2 solubility in basaltic melts (Moore, 1979; Dixon et al., 1995). At the pressures associated with magma storage and crystallisation, even at the Moho, the melts most enriched in CO_2 are likely to be CO_2-oversaturated. An oversaturated melt will tend to return to saturation by degassing CO_2 (Figure 3b). To quantify the solubility of CO_2 in the melts, and therefore their variable extents of degassing, we use the solubility model of Shishkina et al. (2014). In addition to modelling the pressure dependence of CO_2 solubility, Shishkina et al. (2014) also quantify the effect of the major element composition of the melt, through a parameter they call π^*. To retain simplicity in our

models we set π^* to a constant value of 0.34, typical of mid-ocean ridge tholeiites. In detail, π^* will correlate with trace element concentration, even in melts from a single-lithology mantle, as melt major element chemistry correlates with depth and degree of melting (Klein & Langmuir 1987). A variable π^* is, however, a secondary effect to the melting and mixing processes we incorporate in our model. We also assume that melts do not retain supersaturation, which means that our results are conservative estimates for the effect of degassing on preserved CO_2-trace element ratios as some degree of supersaturation is required to drive bubble nucleation (e.g., Bottinga 1990).

A single pressure is chosen for each run of the model, corresponding to the magma storage depth. Melts that have a saturation pressure lower than this retain their initial CO_2 concentration. The most enriched melts may reach CO_2 saturation at greater pressures than the crustal depths used in the models, and therefore may begin degassing before the single degassing stage used in the model. Since CO_2 solubility monotonically decreases with decreasing pressure, even if these melts lose CO_2 during transport they will in all likelihood still arrive oversaturated in CO_2 at the pressure of magma storage. Degassing during transport will never cause the melts to lose more CO_2 than they would during a single (efficient) degassing interval at the pressure of magma storage. The melts are likely to continue mixing and crystallising as they travel upwards through the crust, and therefore may experience many episodes of degassing followed by mixing. Since the melt inclusions that are most likely to preserve mantle CO_2/Ba or CO_2/Nb values are entrapped at the first stage of crystallisation and then remain isolated from the melt, we do not consider subsequent mixing or degassing.

2.3 Mixing Model

The final step in our model is the mixing of the partially degassed melts generated in the previous two steps (Sections 2.1 and 2.2), shown schematically in Figure 3c. In making this the last stage of the model, we are implicitly assuming the timescale of degassing, controlled by bubble nucleation, is faster than the timescale of mixing. We follow the statistical mixing methodology used by Rudge et al. (2013) to model the partial mixing process. Rudge et al. (2013) utilise the properties of the Dirichlet distribution, in particular it has very strong independence properties, meaning that all melts are treated equally according to their relative proportions, denoted as ω_i. A comprehensive description of the model is given by Rudge et al. (2013), and so we provide only a summary here.

A mixed melt of composition $\hat{C}$ is generated by randomly mixing m melt compositions entering the crust, $C^{(i)}$, according to their proportions $\hat{r}_i$:

$$\hat{C} = \sum_{i=1}^{m} \hat{r}_i C^{(i)}$$

where the hats on $\hat{C}$ and $\hat{r}_i$ indicate that they are random variables. The mean composition of the melts entering the crust is fixed by the mass proportion of each melt present, ω_i:

$$\bar{C} = \sum_{i=1}^{m} \omega_i C^{(i)}$$

therefore, to conform with mass balance the expectation value for the proportions of melts going into a mixture, $\hat{r}_i$, is given by:

$$\mathbb{E}(\hat{r}_i) = \omega_i$$

Formally, the proportions that the melts are mixed with are distributed according to a Dirichlet distribution with parameters:

$$\{\hat{r}_1, \hat{r}_2, \dots, \hat{r}_m\} \sim \mathrm{Dir}(\alpha_1, \alpha_2, \dots, \alpha_m)$$

where α_i is related to the mixing parameter, N, by:

$$\alpha_i = (N-1)\omega_i$$

N can range from unity, representing no mixing, to ∞, representing complete mixing. Melts are weighted by ω_i values corresponding to a triangular melting region, i.e. the deepest melts have a greater weighting than more shallow melts. Maclennan (2008) showed that melts in Iceland become increasingly mixed as crystallisation proceeds and the melts become more evolved; Rudge et al. (2013) successfully modelled this by varying the mixing parameter from 12, for the most primitive melts, to 108 for the most evolved. In the models presented here we use a constant mixing parameter of 16, typical of the earliest stages of crystallisation. The effect of the mixing parameter on our results is discussed in Appendix B.

Correlations between CO_2 and trace elements are a primary consideration of this contribution. The properties of the Dirichlet distribution allow calculation of the variance of individual elements, the covariance of two elements, and from these the Pearson correlation coefficient (Rudge et al., 2013). For melts from a single lithology, as modelled here, the variance of a single element, $\hat{C}^{(1)}$, is given by:

$$\mathrm{var}\left(\hat{C}^{(1)}\right) = \frac{1}{N}\sum_{i=1}^{n} \omega_i \left(c_i^{(1)} - \bar{C}^{(1)}\right)^2$$

and the covariance of two elements, $\hat{C}^{(1)}$ and $\hat{C}^{(2)}$, by:

$$\mathrm{cov}\left(\hat{C}^{(1)}, \hat{C}^{(2)}\right), = \frac{1}{N}\sum_{i=1}^{n} \omega_i \left(c_i^{(1)} - \bar{C}^{(1)}\right)\left(c_i^{(2)} - \bar{C}^{(2)}\right)$$

The Pearson correlation coefficient between two elements can be expressed as:

$$\mathrm{cor}\left(\hat{C}^{(1)}, \hat{C}^{(2)}\right) = \frac{\mathrm{cov}\left(\hat{C}^{(1)}, \hat{C}^{(2)}\right)}{\sqrt{\mathrm{var}\left(\hat{C}^{(1)}\right)\mathrm{var}\left(\hat{C}^{(2)}\right)}}$$

since the mixing parameter, N, cancels, the correlation coefficient between two elements is independent of degree of mixing, assuming the remaining range in the element concentrations is significantly above the level of analytical uncertainty.

Whilst it is the correlation between CO_2 and trace elements that has been used to assess the behaviour of CO_2 during melting (and whether it has subsequently degassed), the calculation of the mantle CO_2 concentration assumes direct proportionality between the CO_2 concentration and CO_2/trace element (El) ratios. The behaviour of CO_2/trace element ratios are therefore also of interest. Unfortunately, simple analytical expressions for the variance, covariance and correlation of element ratios at low degrees of mixing do not exist, but can be calculated by drawing a large number of samples from the Dirichlet distribution. Since the variance of a single element ratio and the covariance of two ratios do not depend on the mixing parameter, N, in a simple way, the correlation coefficient between element ratios is also a function of mixing parameter (as shown in Appendix B).

3 Mixing systematics

Before applying the mixing model, qualitative inferences may be drawn about the covariance and correlation between CO_2 and trace elements by considering mixing arrays between end member fractional melts. Firstly, the simplest case is characterised: the correlation between CO_2 and a trace element that behaves identically to CO_2 prior to CO_2 vapour saturation (Section 3.1). This approach is then generalised to the correlation between CO_2 and trace elements with differing compatibility during melting (Section 3.2). Finally, to quantify the correlations between CO_2 and trace elements, the Dirichlet mixing scheme is introduced in Section 3.2. The implications of mixing for apparent similarities in behaviour of CO_2 and trace elements are discussed in Section 3.3. In Section 3.4 the

control degassing pressure exerts on the resulting CO_2-trace element correlations is explored.

3.1 Identical CO_2-trace element partitioning

If a trace element behaves identically to CO_2 during mantle melting and crustal differentiation (prior to CO_2 saturation), concentrations in fractional and variably differentiated melts will describe a straight line passing through the origin when plotted against CO_2 concentration (Figure 3a). The most enriched of these fractional melts will be oversaturated in CO_2 vapour at crustal pressures, and therefore will degas CO_2 until they reach CO_2 saturation (Figure 3b). This degassing process causes the CO_2 concentrations of the most enriched melts to be decoupled from the trace element concentrations, whilst the depleted melts are unaffected.

Mixing of fractional melts may only produce melt compositions lying within the extremes of the unmixed fractional melts. These bounds may coincide with the arrays of primary fractional melts, otherwise they correspond to mixing lines between extreme compositions (Figure 3c). Melts generated by mixing of these fractional melts must therefore lie within the green-shaded area on Figure 3c. When melts originally at CO_2 vapour saturation mix with undersaturated melts, the mixed melts will become undersaturated, since we do not allow π^* to vary. Mixed melts lying within this triangle will define a positive correlation, with an average CO_2/El ratio that will be considerably lower than the mantle CO_2/El ratio. In the next Section, we explore how differing trace element behaviour affects this observation, and in Section 3.4 we show that the average CO_2/El ratio, even for correlated CO_2-El datasets is controlled primarily by the pressure of degassing.

Though the compositional limits of near-fractional melt mixing can be determined very simply using the process described above, the space enclosed by these limits is not inhabited with uniform likelihood. For extents of melting expected at mid-ocean ridges ($\leq$ 15%), most melts are produced at high melt fractions once the residual mantle has already been almost entirely stripped of incompatible trace elements. Due to the overwhelming proportion of depleted fractional melts, mixed melt compositions are biased towards the depleted region. In the Section 3.2 we quantify this phenomenon with the Dirichlet mixing model.

3.2 Generalised CO_2- trace element partitioning

The methodology developed in the preceding section can be generalised to elements with differing compatibilities to CO_2. The primary melts, rather than falling on a straight array, now define a curve (Figure 4a). Little change from the identical partitioning case is seen for trace elements behaving more incompatibility than CO_2, this is due to the residual porosity retained throughout melting, which damps variability in extracted melts when $D_{\mathrm{El}} < \phi$. In addition to the systematics in trace element (El)- CO_2 space, we also show the behaviour in CO_2/El – El space (Figure 4b), and CO_2/El – 1/El space (Figure 4c). Figure 4b may be compared with the data compilation in Figure 2; plotting CO_2/El ratios against 1/El concentrations offers the advantages of linear mixing bounds and an expansion of the region containing maximum CO_2/El observations (the depleted melts; Figure 4c).

The green shading in Figure 4 shows the logarithmic probability distribution of mixed melts, demonstrating that they are biased towards the depleted region of the space, as discussed in Section 3.1. It is immediately apparent from Figure 4a that positive correlations between CO_2 and trace elements are generated from partially degassed

melts. Importantly, the greatest population density of these melts is seen in a narrow array, similar in appearance (but not gradient) to the expectation from a suite of undegassed melts. This feature persists in spite of the broad mixing bounds (green and blue lines) defined by mixing of endmember melt compositions. The gradient of this array is lower than the CO_2/El ratio of the source (Figure 4b and Figure 4c) and the average CO_2/El ratio is much lower than the source CO_2/El ratio (horizontal grey line), although the maximum of the probability distribution does tend towards the source value. In fact, the maximum of the distribution can exceed the source CO_2/El it if the trace element is more incompatible (Figure 4bi), or much more compatible (Figure 4biv) than CO_2. These two scenarios are distinguished from one another by the relation of maximum CO_2/El to El concentration: in the $D_{El} \ll D_{CO2}$ case, CO_2/El of the melts exceeds the source in the most incompatible trace element depleted melts, whereas for $D_{El} \gg D_{CO2}$ case, the most incompatible trace element enriched melts have CO_2/El greater than the source. We discuss the implications of this for identifying mantle CO_2/El values in Section 4.3.

CO_2/El ratios in melts will only reflect the trace element ratio of the source if CO_2 has not been fractionated from the trace element.. Degassing very strongly fractionates CO_2 from all trace elements in melts that are oversaturated at the pressure of magma storage, and significantly reduces the CO_2/El ratio of the most enriched melts. Subsequent mixing between the high, primary, CO_2/El ratio of the trace element depleted endmember with the low, degassed, CO_2/El ratio of the trace element enriched endmember, tends to generate negative correlations in CO_2/El-El space (Figure 4bi-iii) and positive correlations in CO_2/El-1/El space (Figure 4ci-iii). Only for the most compatible elements is the original pre-degassing positive correlation of the CO_2/El-El array, or negative correlation for the CO_2/El-1/El array, retained (Figure 4biv and Figure 4civ). Sufficient concentrations of more compatible elements persist in the residue

during melting such that many of the higher degree primary melts continue to have significant compatible trace element concentrations, whilst having a primary depletion in CO_2. These moderately enriched melts do not saturate in CO_2 vapour and so retain their primary CO_2/El ratio and therefore continue to provide an enriched high CO_2/El mixing endmember.

Since degassing exerts a control on the systematics of data plotted in CO_2/El-1/El space, this behaviour can be used to check for and track any degassing processes that a dataset has experienced. To quantify this behaviour the Pearson correlation coefficient may be used. A coefficient value of 0 indicates no correlation and values of -1 and +1 indicate perfect negative and positive correlations, respectively. The value of the coefficient for the mixed distributions shown in Figure 4 is displayed in the top right-hand corner of each panel. Figure 5 shows how correlations in CO_2-El – 1/El space vary with degassing pressure and trace element partitioning coefficient. When there is no degassing (black line), the transition between positive and negative correlations is rapid, and occurs when the trace element switches from being infinitesimally more incompatible, to infinitesimally more compatible than carbon. When partial degassing has taken place a much smoother transition is seen, and correlations cross from negative to positive at progressively greater trace element partition coefficients as the pressure of degassing decreases. Positive correlations are generated by having many low CO_2/El melts at low 1/El (Figure 4c), these are the most degassed and incompatible trace element enriched melts. As degassing pressure decreases a greater number of melts degas, and the CO_2 they retain decreases; the positive correlation will tend to be enhanced. Negative correlations are generated by decoupling between CO_2 and El during melting and so are most prevalent for the most compatible elements. The partition coefficient at which the transition from positive to negative correlation occurs is

determined by the competition between these two effects, the tendency to observe a positive correlation in CO2/El vs. 1/El space increases with decreasing degassing pressure. The model also makes predictions about the variance in CO2/El with El concentration, however existing datasets do not contain sufficient analyses to accurately estimate these parameters and allow us to test the model.

3.3 Apparent mantle partitioning behaviour from CO_2-trace element correlations

Empirical constraints have been placed on the partitioning behaviour of CO_2 during mantle melting by the degree of correlation between CO_2 and trace elements (Saal et al., 2002; Michael and Graham, 2015; Le Voyer et al., 2017). Saal et al. (2002) and Michael and Graham (2015) find the strongest correlation between CO_2 and Nb, whilst Le Voyer et al. (2017) find CO_2 correlates equally well with Rb, Ba and Nb. Such relationships between carbon and trace elements only directly reflect mantle partitioning behaviour if no degassing has occurred, with the results above showing that positive correlations are readily generated in partially degassed melts (Figure 4).

The behaviour of the correlation coefficient between CO_2 and trace elements as a function of partition coefficient is displayed in Figure 6. When there is no degassing, CO_2 correlates extremely well with the most incompatible elements; the lack of variation in correlation coefficient for the most incompatible elements arises from the residual porosity during melting (i.e., our use of a continuous melting model as opposed to pure fractional). The correlation coefficient between CO_2 and trace elements then decreases with increasing trace element compatibility (Figure 6, black line).

In contrast, when partially degassed melts are mixed, the correlation coefficient does not decrease monotonically as the reference trace element becomes increasingly compatible. Instead, mixing of degassed melts creates a maximum in correlation

coefficient centred on a higher (i.e. more compatible) partition coefficient than CO_2 (Figure 6). This pattern is also present in the synthetic data presented in Figure 4aiii, which shows data lying within a tight wedge. This result owes to a smaller range in trace element concentrations being generated when the trace element D is high. Model runs shown in Figure 7, where CO_2 is plotted against Ba, and Figure 8, where CO_2 is plotted against Nb, show how better correlations may be developed between CO_2 and Nb, rather than CO_2 and Ba, despite the carbon partition coefficient used in the models being closer in value to Ba (Rosenthal et al., 2015).

3.4 Effect of degassing pressure

The CO_2/El ratios of the melts generated by the model are controlled by mixing between a trace element depleted, but high, primary, CO_2/El endmember, and a trace element enriched, but low, degassed, CO_2/El endmember. The value of the low CO_2/El endmember is determined by the CO_2 content of the melts at saturation, which is controlled by pressure. Reducing the pressure of degassing has the effect of rotating the array in CO_2-trace element space to shallower slopes (Figure 7 and Figure 8).

The mantle CO_2/Nb ratio has often been constrained by fitting a line through the data in CO_2-trace element space. This process should be carried out using orthogonal distance regression, since neither variable is strictly dependent. We fit an equation of the form:

$$f(\mathrm{El}) = m \cdot \mathrm{El}$$

where El is the concentration of the trace element, and m is varied so that the misfit between CO_2 and $f(\mathrm{El})$ is minimised. The parameter m corresponds to the best fit CO_2/El ratio. Calculations were performed using the ODRPACK library (Brown and Fuller, 1990) with the SciPy interface (Jones et al., 2014). The results of these calculations are shown

by the red dashed lines in Figure 7 and Figure 8, and the values of the best fit CO_2/El ratio are shown in the top right corner of each panel. Any amount of degassing reduces the CO_2/El ratio inferred by this method, despite an apparently good fit to the data in CO_2-trace element space. As the number of draws from the distribution increases, the best fit ratio will tend towards the mean ratio of the starting melts.

3.5 Effect of analytical uncertainty

Using plots where one variable appears in the expressions plotted on both x and y axes can lead to the appearance of spurious correlations (Jackson and Somers, 1991). Analytical error in El concentration will not only affect the concentration of El (or 1/El) plotted on the x axis, but also the value of CO2/El plotted on the y axis. Measurements of trace element and CO2 concentrations in melt inclusions generally have uncertainties ~10% (Saal et al., 2002; Le Voyer et al., 2017), the vector that describes the effect of this uncertainty is shown by the black lines and circles in Figure 2c and 2d. In the datasets considered here the signal is much greater than the analytical uncertainty.

4 Implications for existing datasets

In Section 3.2 we demonstrated that positive correlations between CO_2 and trace elements are not a unique property of undegassed melts. Published datasets that have utilised the presence of CO_2-trace element correlations as a criterion for identifying the absence of degassing must, therefore, be reassessed.

4.1 Signatures of partial degassing in nominally undegassed sample suites

Since degassing only affects the melts that have the highest concentrations of CO_2, additional structure is introduced into the data: rather than almost horizontal arrays in CO_2/Ba-Ba space, partially degassed melts will exhibit negative correlations. Figure 2c

444 demonstrates that the data from Siqueiros, Northern Iceland, Equatorial Atlantic and the
445 undersaturated D-MORB glasses all exhibit these negative correlations between CO_2/Ba
446 and Ba. Furthermore, if CO_2 has not degassed prior to inclusion entrapment, the
447 correlation coefficient between CO_2/El and 1/El should reverse sign as trace elements go
448 from being more incompatible to more compatible than CO_2 during melting (Figure 5).
449 The data from both Siqueiros and Equatorial Atlantic retain a positive correlation far
450 beyond the experimental CO_2 partition coefficient (Rosenthal et al., 2015), and beyond
451 Nb which CO_2 has been likened to empirically (Saal et al., 2002). This decoupling between
452 the apparent partition coefficients of C and trace elements in all these datasets also
453 suggests that they have experienced partial degassing.

454 At higher values of trace element D, the correlation coefficients between CO_2/El
455 and 1/El calculated from the published data departs from the predicted behaviour
456 (Figure 5b). This departure is likely to arise from the behaviour of these elements during
457 garnet-field melting or fractional crystallisation. When garnet is in the residue, the bulk
458 partition coefficients during mantle melting increase significantly. This variation can be
459 modelled with the alphaMELTS frontend (Smith and Asimow, 2005) to the pMELTS
460 thermodynamic model (Ghiorso et al., 2002), and the resulting correlations are shown in
461 Figure 5 (dashed lines, calculation details given in figure caption). Garnet-field melting
462 can account for this discrepancy, though we do not rule out the role of fractional
463 crystallisation.

464 The undersaturated glass dataset, shown in Figure 1 and 2, displays CO_2 co-
465 variation with both Ba and Nb; additionally, and a negative correlation between CO_2/Ba
466 and Ba. These properties are consistent with the partial degassing and mixing model
467 despite the dataset not representing co-genetic melts. The partial degassing and mixing
468 process may still be controlling the systematics of this dataset if the glasses are derived

from melts sampling sources with the same CO_2/Ba, but with different proportions of low and high degree melts, and mixing occurring at similar pressures. Whilst this uniformity is not ubiquitous in the global mid-ocean ridge system, it may well be present when only undersaturated glasses are considered. Alternatively, varying mantle Ba concentration, at near-constant CO_2 concentration, could generate the observed covariation between CO_2/Ba and Ba concentrations in the glasses.

Previous studies have interpreted melt inclusions from the Siqueiros fracture zone to be near primary melts, having undergone negligible mixing and fractionation within the crust (Perfit et al., 1996). However, the CO_2- trace element systematics are difficult to explain without the partial degassing and mixing processes. The Siqueiros melts are very depleted in trace elements. Furthermore, whilst the trace element data might be matched by batch melting models, it does not preclude their origin from mixing of more variable fractional melts. U-Series disequilibria provide support for fractional melting, indicating that Siqueiros fracture zone melts segregated from their residue at small porosities in a process that must therefore have been near-fractional (Lundstrom et al., 1999). Recent seismic evidence suggests axial magma chambers are present beneath ultra-slow spreading ridges (Jian et al., 2017). Therefore, despite the lower rates of magma supply, these slow spreading systems nonetheless retain melt that new primitive magmas may interact with during their transport and storage in the crust.

4.2 Global mantle CO_2 heterogeneity

Substantial heterogeneity in the CO_2/Nb and CO_2/Ba ratios of the depleted mantle has been inferred from the variation in averages of these ratios, obtained by fitting lines though data in CO_2-Ba and CO_2-Nb space from Siqueiros, Northern Iceland and the Equatorial Atlantic. For the reasons outlined above, the inclusions measured in these

493 studies are all likely to be preserving partially degassed melts. When partial degassing
494 and mixing has taken place the apparent ratio in CO_2-Ba and CO_2-Nb space is determined
495 not by the primary mantle ratios, but by the degassing pressure (Section 3.4). Instead,
496 the best estimate of mantle CO2 concentration comes from the maximum ratio CO_2/Ba
497 ratio recorded by the most trace element depleted melts in the dataset; these melts are
498 the most likely to have remained CO_2 undersaturated (Section 3.2). The maximum
499 CO_2/Ba ratios observed in melt inclusions from Siqueiros and Northern Iceland, and the
500 undersaturated D-MORB glasses, are all ~140 (with a maximum value of 146). If this
501 observed maximum ratio is close to the real maximum of the distributions of mixed melts,
502 then it suggests all three datasets are consistent with a single depleted mantle CO_2/Ba
503 ratio. Furthermore, apart from one extreme outlier, the maximum CO_2/Ba ratios in melt
504 inclusions from Axial Seamount (Helo et al., 2011) and Gakkel Ridge (Shaw et al., 2010;
505 Wanless et al., 2014) are consistent with this (Figure 1). In contrast, the maximum
506 CO_2/Ba ratio observed in the Equatorial Atlantic melt inclusions is 107. This could be
507 reconciled either by the Equatorial Atlantic dataset not adequately characterising the
508 maximum CO_2/Ba ratio in the distribution, or by localised mantle CO_2/Ba heterogeneity
509 as might be expected given the presence of Ba/Nb heterogeneity in the MORB source
510 (Michael and Graham, 2015). Though small-scale mantle heterogeneity has been
511 observed in both the MORB and Iceland mantle sources, linking this to volatile elements
512 such as carbon is intrinsically difficult owing to a bias in preserving the CO_2/Ba ratios of
513 only the most depleted melts.

514 An alternative possibility to the model we have developed here is that diversity in
515 melt CO_2/Ba and CO_2/Nb arises from mantle CO_2/Ba and CO_2/Nb heterogeneity. Melting
516 of such a heterogeneous mantle must produce both a high CO_2/Ba, low Ba component,
517 and a low CO_2/Ba, high Ba component. For the observed negative correlations between

CO_2/Ba and Ba to be generated, a low CO2/Ba, low Ba component cannot be involved in mixing. However, generating such melts is a natural consequence of melting mantle heterogeneities beyond the smallest of melt fractions, at which point even enriched lithologies are depleted in highly incompatible elements such as Ba. Therefore, mantle heterogeneity alone is highly unlikely to account for the observed correlations.

4.3 Constraining mantle CO_2/Ba

In a partially degassed dataset, the CO_2/Ba measurement most likely to represent the mantle CO_2/Ba ratio is the maximum ratio observed. A disadvantage of utilising maxima in geochemical datasets is that they are strongly dependent on sample size. For melts to preserve high CO_2/Ba they must have minimal interaction with degassed melts. Depending on the diversity of melts entering magma storage regions, only a small proportion of melts may retain their primary CO_2/Ba. It is therefore most pragmatic to consider the likelihood of melts retaining a CO_2/Ba ratio within 10% of the mantle value.

Figure 9 shows the minimum number of melt inclusion analyses (or here, Dirichlet distributed draws from a population of synthetic melts) required for the maximum CO_2/Ba ratio measured to be within 10% of the mantle value (with >99.8% certainty), for a melting column typical of normal mid-ocean ridges. Since Siqueiros has been identified as sampling ultra-depleted mantle, Figure 9b demonstrates how the minimum number of analyses changes if trace element concentrations are more depleted in the mantle source (Workman and Hart, 2005). At constant source CO_2/Ba ratio, a source more depleted in trace elements will produce melts that are, on average, less CO_2 rich, and therefore more likely to retain their primary CO_2/Ba ratio. The number of analyses required increases as degassing pressure decreases and mantle CO_2/Ba increases; both these changes cause the proportion of melts degassing CO_2 to increase, therefore increasing the likelihood of

an undegassed melt mixing with degassed melt and thus erasing the signal of primary CO_2/Ba from the population of melts. In addition, the value of the mixing parameter will affect the position of the contours in Figure 9, with greater degrees of mixing making observing mantle CO_2/Ba less likely. Making large numbers of analyses on melt inclusions trapped at high pressure offers the greatest prospect of observing the mantle CO_2/Ba ratio.

Both the Borgarhraun and Siqueiros datasets consist of around 100 melt inclusion analyses each (Figure 9a). Provided these inclusions were trapped at sufficient pressure, the maximum CO_2/Ba they record is likely to be very close to the mantle value. However, the Mid-Atlantic dataset consists of 21 melt inclusion analyses only (Figure 9a). Barometry indicates crystallisation takes place at pressures as high as 10 kbar beneath the Mid-Atlantic ridge, though erupted liquids predominantly equilibrate at lower pressures (Herzberg, 2004). If the Mid-Atlantic dataset is also sampling a mantle of CO_2/Ba = 140, Figure 9 suggests the maximum observed CO_2/Ba ratio will only preserve the mantle value if inclusions were entrapped at the deepest extents of crystallisation (> 8 kbar). Therefore, the Mid-Atlantic dataset may also be consistent with a mantle CO_2/Ba ratio of 140.

Assuming a Ba concentration in the depleted mantle of 0.563 ppm (Workman and Hart, 2005), a CO_2/Ba ratio of 140 ppm implies a mantle CO_2 content of 79 ppm, more than double that inferred by Workman and Hart (2005) from the canonical CO_2/Nb ratio (Saal et al., 2002). Rosenthal et al. (2015) reach a similar conclusion, and also discuss the likely CO_2 content of mantle melting beneath intra-plate volcanoes.

4.4 Origin of CO_2 undersaturation

Both the Siqueiros melt inclusions and undersaturated mid-ocean ridge glass datasets record CO_2 concentrations that are undersaturated at the pressure of eruption, and the CO_2 concentrations present in the Equatorial Atlantic dataset would be undersaturated at during crystallisation within the oceanic crust. This CO_2 undersaturation has been used as further evidence for the absence of degassing (Saal et al., 2002; Michael and Graham, 2015). Though the mixing-degassing model requires some of the fractional melts to become CO_2 saturated, they subsequently mix with highly CO_2 undersaturated melts, resulting in all melts becoming undersaturated at the pressure of degassing (Figure 7). If a sufficient mass of depleted melts are present, this undersaturation may be retained at the pressure of eruption, as in the Siqueiros and undersaturated mid-ocean ridge glass datasets, even with mixing in of enriched low CO2/En melts having occurred.

5 Conclusions

CO_2 concentrations in melt inclusions provide an important constraint on global CO_2 flux from the mantle at mid-ocean ridges and ocean islands and are vital for assessing CO_2 heterogeneity in the mantle. Melt inclusion datasets are a key petrological tool for addressing these problems, and in this study we have formalised the robustness of the melt inclusion archive to the common magmatic processes of mixing and degassing.

We have identified how trace elements co-vary with CO_2 in melts, following mixing of trace element depleted CO_2 undersaturated melts with trace element enriched CO_2 saturated melts. We show that when degassing occurs, CO_2 may have a stronger correlation with Nb, even if its partitioning behaviour during melting is more similar to Ba (Rosenthal et al., 2015). We find that the average CO_2/Ba ratio in a melt inclusion

dataset is dominated by the pressure of degassing, rather than the mantle CO_2/Ba ratio. The best estimate of mantle CO_2/Ba ratio is, instead, the maximum CO_2/Ba ratio observed.

Comparison of the model results with CO_2-undersaturated D-MORB glasses (Michael and Graham, 2015), and melt inclusion datasets from Northern Iceland (Hauri et al., 2002), Siqueiros (Saal et al., 2002) and the Equatorial Atlantic (Le Voyer et al., 2017), suggests these datasets all record CO_2 concentrations generated by mixing of partially degassed melts (Section 4). We argue that the available datasets are all consistent with a depleted mantle CO_2/Ba of ~140, and do not require heterogeneity in mantle CO_2/Ba.

The role of mixing in the generation of melts trapped in melt inclusions has been neglected in the interpretation of CO_2 concentrations, leading to underestimation of the CO_2 content of the mantle and inferences of CO_2 heterogeneity. Despite the likely presence of partial degassing in all melt inclusion datasets, fully characterising the maxima of CO_2/Ba values by making many melt inclusion analyses may allow the mantle CO_2/Ba ratio to be extracted from the data. Subject to the assumptions of our simple melting and mixing models, we can estimate the likelihood of recovering mantle CO_2/Ba in melt inclusion datasets, a result which is useful in preparing analytical studies.

6 Acknowledgements

The authors would like to thank the Isaac Newton Institute for Mathematical Sciences for its hospitality during the programme 'Melt in the Mantle', which was supported by EPSRC Grant Number EP/K032208/1. SM was supported by a Natural Environment Research Council Studentship NE/L002507/1 and NE/M000427/1. OS thanks Trinity College Cambridge for support through a Title A Fellowship. JFR thanks

612 the Leverhulme Trust. Raj Dasgupta and an anonymous reviewer are thanked for their
613 constructive comments which helped improve the manuscript. Frederic Moynier is
614 thanked for his editorial handling.

615 7 References

616 Bianchi, D., Sarmiento, J.L., Gnanadesikan, A., Key, R.M., Schlosser, P., Newton, R., 2010.
617 Low helium flux from the mantle inferred from simulations of oceanic helium isotope
618 data. Earth Planet. Sci. Lett. 297, 379–386.
619 Boudier, F., Nicolas, A., Ildefonse, B., 1996. Magma chambers in the Oman ophiolite: fed from
620 the top and the bottom. Earth Planet. Sci. Lett. 144, 239–250.
621 Brown, P.J., Fuller, W.A., 1990. Statistical Analysis of Measurement Error Models and
622 Applications: Proceedings of the AMS-IMS-SIAM Joint Summer Research Conference
623 Held June 10-16, 1989, with Support from the National Science Foundation and the US
624 Army Research Office. American Mathematical Soc.
625 Cartigny, P., Pineau, F., Aubaud, C., Javoy, M., 2008. Towards a consistent mantle carbon flux
626 estimate: Insights from volatile systematics (H 2 O/Ce, δD, CO 2/Nb) in the North
627 Atlantic mantle (14 N and 34 N). Earth Planet. Sci. Lett. 265, 672–685.
628 Craig, H., Clarke, W.B., Beg, M.A., 1975. Excess 3He in deep water on the East Pacific Rise.
629 Earth Planet. Sci. Lett. 26, 125–132.
630 Dasgupta, R., 2013. Ingassing, storage, and outgassing of terrestrial carbon through geologic
631 time. Rev. Mineral. Geochemistry 75, 183–229.
632 Dasgupta, R., Hirschmann, M.M., 2010. The deep carbon cycle and melting in Earth's interior.
633 Earth Planet. Sci. Lett. 298, 1–13.
634 Dixon, E.J., Stolper, E.M., Holloway, J.R., 1995. An Experimental Study of Water and Carbon
635 Dioxide Solubilities in Mid-Ocean Ridge Basaltic Liquids. Part I: Calibration and
636 Solubility Models. J. Petrol. 36, 1607–1631.

637 Eguchi, J., Dasgupta, R., 2017. CO2 content of andesitic melts at graphite-saturated upper
638 mantle conditions with implications for redox state of oceanic basalt source regions and
639 remobilization of reduced carbon from subducted eclogite. Contrib. to Mineral. Petrol.
640 172, 12.
641 Ghiorso, M.S., Hirschmann, M.M., Reiners, P.W., Kress, V.C., 2002. The pMELTS: A
642 revision of MELTS for improved calculation of phase relations and major element
643 partitioning related to partial melting of the mantle to 3 GPa. Geochemistry, Geophys.
644 Geosystems 3, 1–35. doi:10.1029/2001GC000217
645 Hauri, E., Gronvold, K., Oskarsson, N., McKenzie, D., 2002. Abundance of carbon in the
646 Icelandic mantle: constraints from melt inclusions, in: AGU Spring Meeting Abstracts. p.
647 3.
648 Hayes, J.M., Waldbauer, J.R., 2006. The carbon cycle and associated redox processes through
649 time. Philos. Trans. R. Soc. London B Biol. Sci. 361, 931–950.
650 Helo, C., Longpré, M.-A., Shimizu, N., Clague, D.A., Stix, J., 2011. Explosive eruptions at
651 mid-ocean ridges driven by CO2-rich magmas. Nat. Geosci. 4, 260–263.
652 Herzberg, C., 2004. Partial crystallization of mid-ocean ridge basalts in the crust and mantle.
653 J. Petrol. 45, 2389–2405.
654 Hirschmann, M.M., Dasgupta, R., 2009. The H/C ratios of Earth's near-surface and deep
655 reservoirs, and consequences for deep Earth volatile cycles. Chem. Geol. 262, 4–16.
656 Hirschmann, M.M., Stolper, E.M., 1996. A possible role for garnet pyroxenite in the origin of
657 the "garnet signature" in MORB. Contrib. to Mineral. Petrol. 124, 185–208.
658 Jackson, D.A., Somers, K.M., 1991. The spectre of "spurious" correlations. Oecologia 86, 147–
659 151.
660 Javoy, M., Pineau, F., 1991. The volatiles record of a "popping" rock from the Mid-Atlantic
661 Ridge at 14 N: chemical and isotopic composition of gas trapped in the vesicles. Earth

662 Planet. Sci. Lett. 107, 598–611.
663 Jian, H., Chen, Y.J., Singh, S.C., Li, J., Zhao, M., Ruan, A., Qiu, X., 2017. Seismic structure
664 and magmatic construction of crust at the ultraslow-spreading Southwest Indian Ridge at
665 50° 28'E. J. Geophys. Res. Solid Earth 122, 18–42.
666 Jones, E., Oliphant, T., Peterson, P., 2014. {SciPy}: open source scientific tools for {Python}.
667 Kasting, J.F., Whitmire, D.P., Reynolds, R.T., 1993. Habitable zones around main sequence
668 stars. Icarus 101, 108–128.
669 Katz, R.F., Spiegelman, M., Langmuir, C.H., 2003. A new parameterization of hydrous mantle
670 melting. Geochemistry, Geophys. Geosystems 4.
671 Kelemen, P.B., Hirth, G., Shimizu, N., Spiegelman, M., Dick, H.J., 1997a. A review of melt
672 migration processes in the adiabatically upwelling mantle beneath oceanic spreading
673 ridges. Philos. Trans. R. Soc. London. Ser. A Math. Phys. Eng. Sci. 355, 283 LP-318.
674 Kelemen, P.B., Koga, K., Shimizu, N., 1997b. Geochemistry of gabbro sills in the crust-mantle
675 transition zone of the Oman ophiolite: Implications for the origin of the oceanic lower
676 crust. Earth Planet. Sci. Lett. 146, 475–488.
677 Kelemen, P.B., Manning, C.E., 2015. Reevaluating carbon fluxes in subduction zones, what
678 goes down, mostly comes up. Proc. Natl. Acad. Sci. 112, E3997–E4006.
679 Le Voyer, M., Kelley, K.A., Cottrell, E., Hauri, E.H., 2017. Heterogeneity in mantle carbon
680 content from CO2-undersaturated basalts. Nat. Commun. 8, 14062.
681 Lundstrom, C.C., Sampson, D.E., Perfit, M.R., Gill, J., Williams, Q., 1999. Insights into mid-
682 ocean ridge basalt petrogenesis: U-series disequilibria from the Siqueiros Transform,
683 Lamont Seamounts, and East Pacific Rise. J. Geophys. Res. Solid Earth 104, 13035–
684 13048.
685 Maclennan, J., 2008. Concurrent mixing and cooling of melts under Iceland. J. Petrol. 49,
686 1931–1953.

687 Maclennan, J., McKenzie, D., Gronvold, K., Shimizu, N., Eiler, J.M., Kitchen, N., 2003. Melt
688 mixing and crystallization under Theistareykir, northeast Iceland. Geochemistry,
689 Geophys. Geosystems 4, 8624.
690 Maclennan, J., McKenzie, D., Gronvöld, K., Slater, L., 2001. Crustal accretion under northern
691 Iceland. Earth Planet. Sci. Lett. 191, 295–310.
692 Marty, B., 2012. The origins and concentrations of water, carbon, nitrogen and noble gases on
693 Earth. Earth Planet. Sci. Lett. 313, 56–66.
694 Matthews, S., Shorttle, O., Maclennan, J., 2016. The temperature of the Icelandic mantle from
695 olivine-spinel aluminum exchange thermometry. Geochemistry, Geophys. Geosystems
696 17, 4725–4752.
697 McKenzie, D., O'Nions, R.K., 1995. The Source Regions of Ocean Island Basalts. J. Petrol.
698 36, 133–159.
699 McKenzie, D., O'Nions, R.K., 1991. Partial Melt Distributions from Inversion of Rare Earth
700 Element Concentrations. J. Petrol. 32, 1021–1091.
701 Michael, P.J., Graham, D.W., 2015. The behavior and concentration of CO2 in the suboceanic
702 mantle: Inferences from undegassed ocean ridge and ocean island basalts. Lithos 236,
703 338–351. doi:10.1016/j.lithos.2015.08.020
704 Moore, J.G., 1979. Vesicularity and CO2 in mid-ocean ridge basalt. Nature 282, 250–253.
705 Neave, D.A., Putirka, K.D., 2017. A new clinopyroxene-liquid barometer, and implications for
706 magma storage pressures under Icelandic rift zones. Am. Mineral. 102, 777–794.
707 Perfit, M.R., Fornari, D.J., Ridley, W.I., Kirk, P.D., Casey, J., Kastens, K.A., Reynolds, J.R.,
708 Edwards, M., Desonie, D., Shuster, R., 1996. Recent volcanism in the Siqueiros transform
709 fault: picritic basalts and implications for MORB magma genesis. Earth Planet. Sci. Lett.
710 141, 91–108.
711 Resing, J.A., Lupton, J.E., Feely, R.A., Lilley, M.D., 2004. CO 2 and 3 He in hydrothermal

712 plumes: implications for mid-ocean ridge CO 2 flux. Earth Planet. Sci. Lett. 226, 449–
713 464.
714 Rosenthal, A., Hauri, E.H., Hirschmann, M.M., 2015. Experimental determination of C, F, and
715 H partitioning between mantle minerals and carbonated basalt, CO2/Ba and CO2/Nb
716 systematics of partial melting, and the CO2 contents of basaltic source regions, Earth and
717 Planetary Science Letters. doi:10.1016/j.epsl.2014.11.044
718 Rudge, J.F., Maclennan, J., Stracke, A., 2013. The geochemical consequences of mixing melts
719 from a heterogeneous mantle. Geochim. Cosmochim. Acta 114, 112–143.
720 Saal, A.E., Hauri, E.H., Langmuir, C.H., Perfit, M.R., 2002. Vapour undersaturation in
721 primitive mid-ocean-ridge basalt and the volatile content of Earth's upper mantle. Nature
722 419, 451–455. doi:10.1038/nature01073
723 Shaw, A.M., Behn, M.D., Humphris, S.E., Sohn, R.A., Gregg, P.M., 2010. Deep pooling of
724 low degree melts and volatile fluxes at the 85 E segment of the Gakkel Ridge: Evidence
725 from olivine-hosted melt inclusions and glasses. Earth Planet. Sci. Lett. 289, 311–322.
726 Shimizu, K., Saal, A.E., Myers, C.E., Nagle, A.N., Hauri, E.H., Forsyth, D.W., Kamenetsky,
727 V.S., Niu, Y., 2016. Two-component mantle melting-mixing model for the generation of
728 mid-ocean ridge basalts: Implications for the volatile content of the Pacific upper mantle.
729 Geochim. Cosmochim. Acta 176, 44–80. doi:10.1016/j.gca.2015.10.033
730 Shishkina, T.A., Botcharnikov, R.E., Holtz, F., Almeev, R.R., Jazwa, A.M., Jakubiak, A.A.,
731 2014. Compositional and pressure effects on the solubility of H 2 O and CO 2 in mafic
732 melts. Chem. Geol. 388, 112–129.
733 Shorttle, O., Rudge, J.F., Maclennan, J., Rubin, K.H., 2016. A Statistical Description of
734 Concurrent Mixing and Crystallization during MORB Differentiation: Implications for
735 Trace Element Enrichment. J. Petrol. 57, 2127–2162.
736 Smith, P.M., Asimow, P.D., 2005. Adiabat_1ph: A new public front-end to the MELTS,

pMELTS, and pHMELTS models. Geochemistry, Geophys. Geosystems 6, n/a-n/a. doi:10.1029/2004GC000816

Sobolev, A. V, 1996. Melt inclusions in minerals as a source of principle petrological information. Petrology 4, 209–220.

Sobolev, A. V, Gurenko, A.A., Shimizu, N., 1994. Ultra-depleted melts from Iceland: data from melt inclusion studies. Miner. Mag A 58, 860–861.

Spiegelman, M., Kelemen, P.B., 2003. Extreme chemical variability as a consequence of channelized melt transport. Geochemistry, Geophys. Geosystems 4.

Walker, J.C.G., Hays, P.B., Kasting, J.F., 1981. A negative feedback mechanism for the long-term stabilization of Earth's surface temperature. J. Geophys. Res. Ocean. 86, 9776–9782.

Wanless, V.D., Behn, M.D., Shaw, A.M., Plank, T., 2014. Variations in melting dynamics and mantle compositions along the Eastern Volcanic Zone of the Gakkel Ridge: insights from olivine-hosted melt inclusions. Contrib. to Mineral. Petrol. 167, 1–22.

Winpenny, B., Maclennan, J., 2011. A partial record of mixing of mantle melts preserved in Icelandic phenocrysts. J. Petrol. 52, 1791–1812.

Workman, R.K., Hart, S.R., 2005. Major and trace element composition of the depleted MORB mantle (DMM). Earth Planet. Sci. Lett. 231, 53–72.

Zou, H., 2007. Quantitative geochemistry. World Scientific.

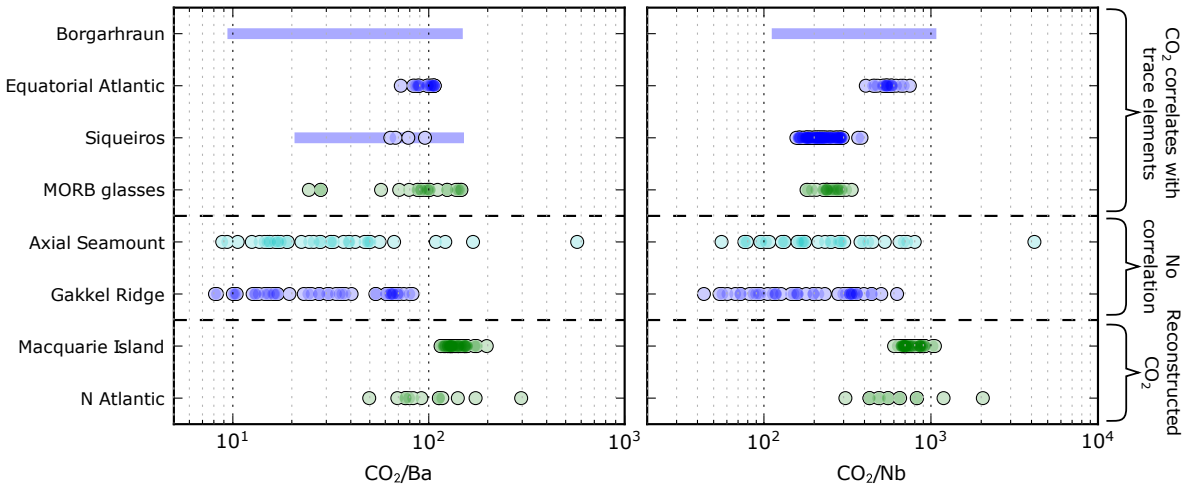

Figure 1. Compilation of published data used for estimating mantle CO_2/Ba and CO_2/Nb ratios. The data are separated into datasets that show a correlation between CO_2 and trace elements (and have therefore been identified as undegassed on that basis), datasets that show no such correlation (and so have been inferred to be partially degassed), and datasets where the CO_2 concentration has been reconstructed from Cl concentrations or C-isotope fractionation. Green points indicate data obtained from glasses, cyan points indicate data obtained from plagioclase hosted melt inclusions, and green indicates data obtained from olivine hosted melt inclusions. Bars indicate unpublished data reported by Rosenthal et al. (2015). Data sources: Borgarhraun (Northern Iceland): unpublished data from Hauri et al., reported by Rosenthal et al. (2015); Equatorial Atlantic: Le Voyer et al. (2017); Siqueiros: Saal et al. (2002), unpublished Ba data from Saal et al. reported by Rosenthal et al. (2015); MORB (undersaturated) glasses: Michael and Graham (2015), Shimizu et al. (2016); Axial Seamount: Helo et al. (2011); Gakkel Ridge: Shaw et al. (2010), Wanless et al. (2014); Macquarie Island: Shimizu et al. (2016); N. Atlantic: Cartigny et al. (2008).

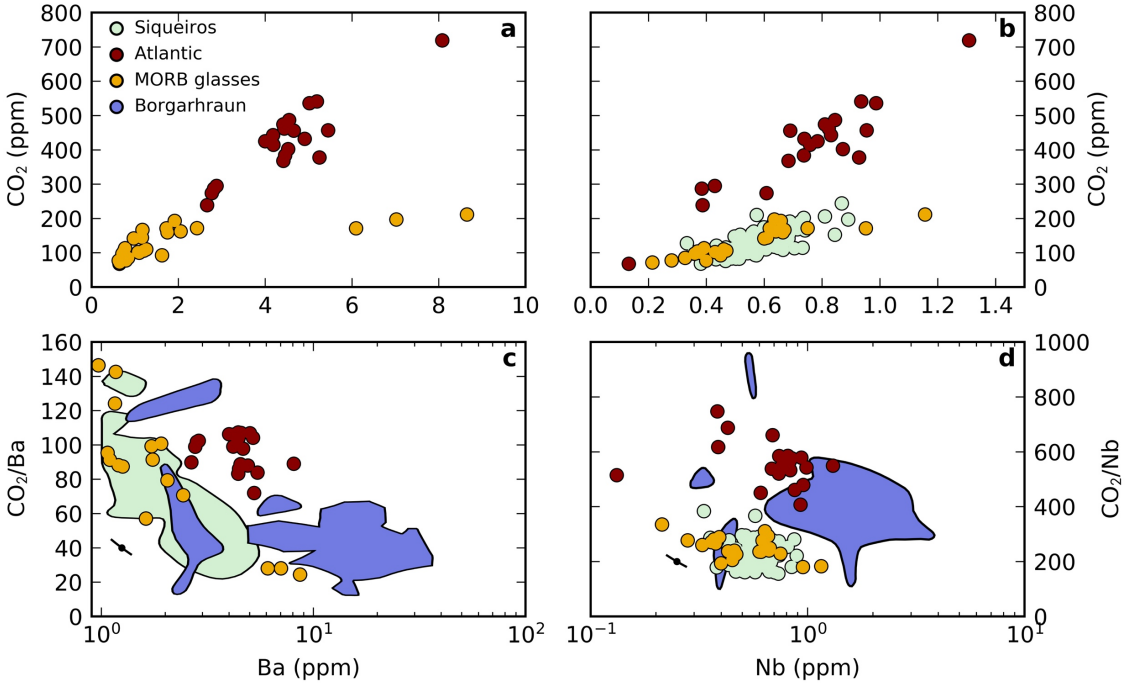

774

775 Figure 2. Compilation of Ba, Nb and CO_2 data for mid-ocean ridge melt inclusion and glass
776 datasets reported as being undegassed. Modified from Rosenthal et al. (2015). Data
777 sources: Siqueiros Nb: Saal et al. (2002); Siqueiros Ba: Saal et al. unpublished data
778 reported by Rosenthal et al. (2015); Atlantic: Le Voyer et al. (2017); MORB glasses:
779 Michael et al. (2015) and Shimizu et al. (2016); Borgarhraun (Northern Iceland): Hauri et
780 al. unpublished data reported by Rosenthal et al. (2015). The black lines and circles in
781 panels c and d show how a 10% uncertainty in Ba or Nb concentration could cause a
782 spurious negative correlation to develop, this effect is much smaller than the signal
783 shown by the datasets. Error in CO2 measurements will cause vertical displacement of
784 the data points only.

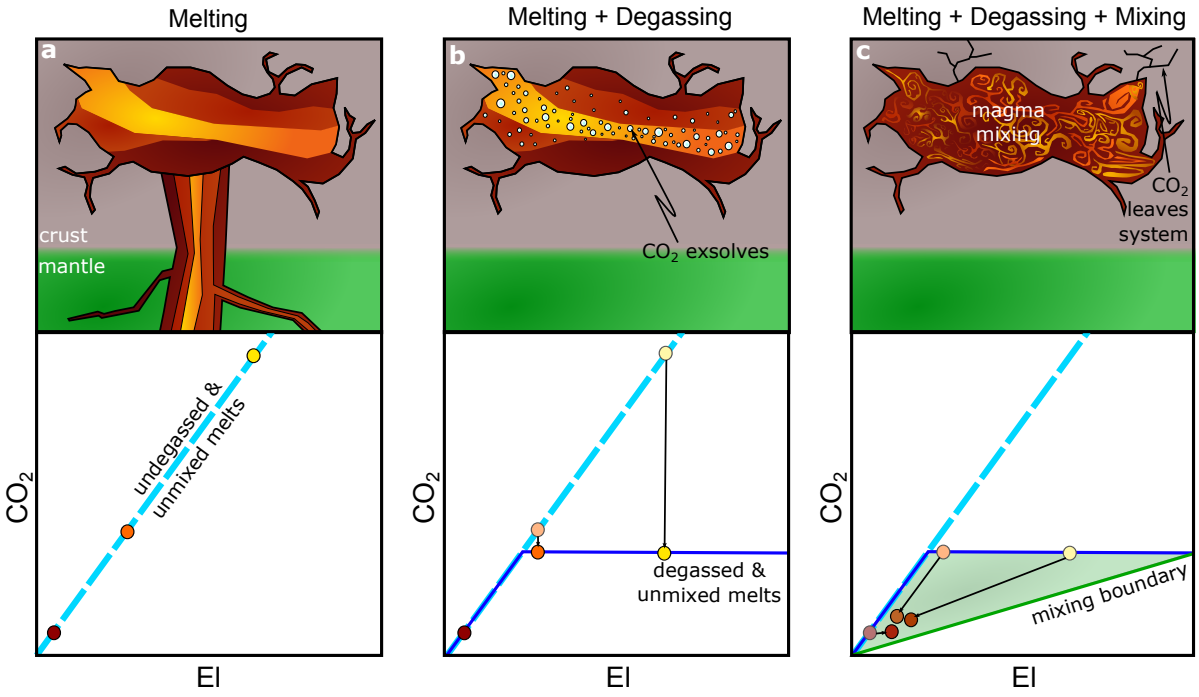

785

786 Figure 3. Cartoons showing how the mixing and degassing calculations proceed. 'El'
787 represents a trace element which behaves identically to CO_2 during mantle melting. In
788 the lower panels, the circles show schematically the behaviour of individual melts
789 throughout the process, whilst the lines show the behaviour of a continuous distribution
790 of melt compositions. The blue dashed line shows the undegassed and unmixed melts
791 (panel a), the solid blue line shows the degassed and unmixed melts (panel b), and the
792 shaded green region (panel c) shows the region between mixing bounds (the solid blue
793 lines and green line). The positions of the solid blue and green lines are determined by
794 the magma storage pressure.

795

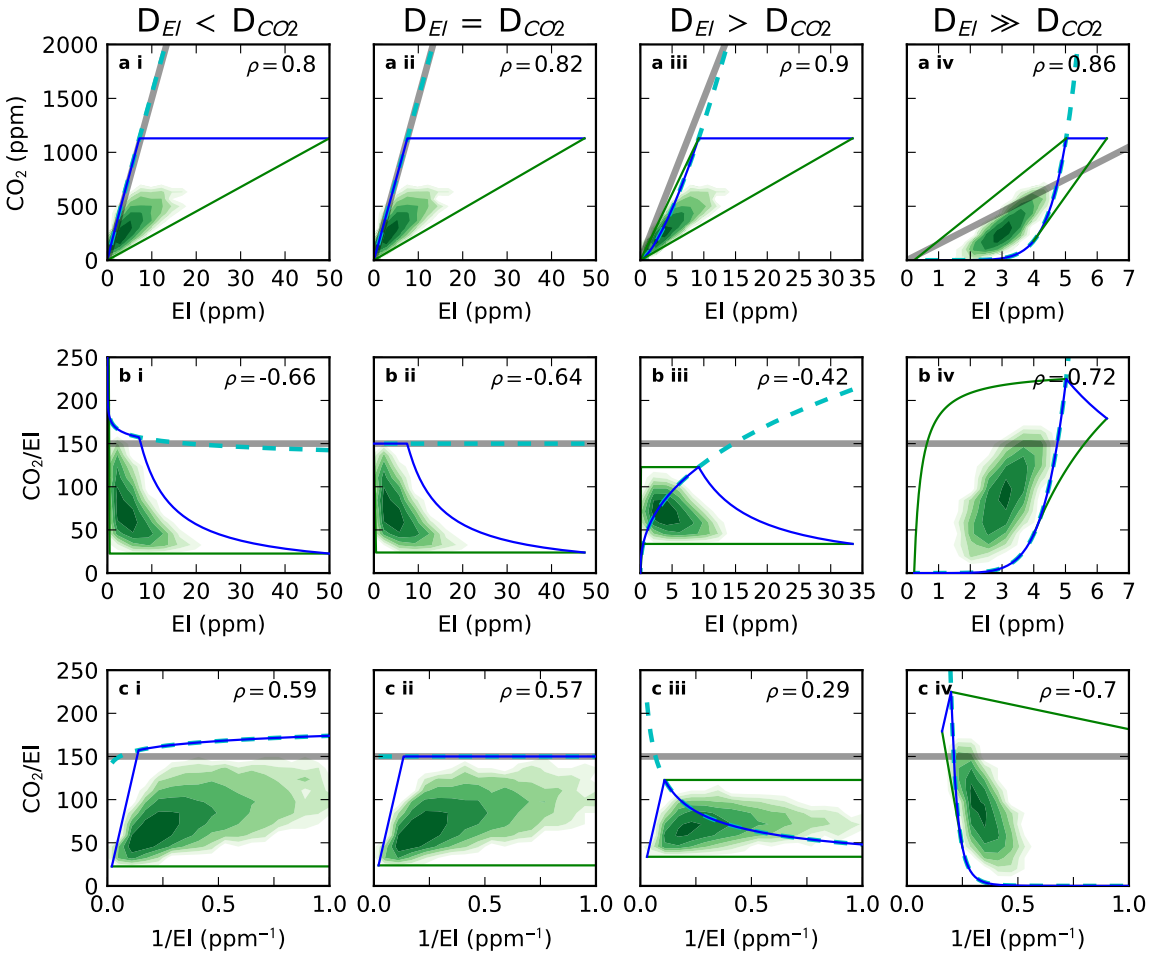

Figure 4. Systematics for trace elements with varying compatibility relative to CO2 (column headings) according to our mixing and degassing model. Trace element concentrations in the solid mantle are set to 0.5 ppm. Each row represents a different way of plotting the systematics, as indicated by the axes labels. See Figure 3 for descriptions of each line. Undegassed and unmixed melts are represented by the cyan dashed line. Degassed and unmixed melts are represented by the solid blue line. The boundaries of the space that can be inhabited by mixed melts are shown by solid green lines, in addition to the solid blue lines. The grey band represents the CO_2/El ratio of the mantle source. The shading represents the logarithmic density of mixed melts generated by the model. The Pearson correlation coefficient (ρ) for the mixed distribution is shown in the upper right hand corner of each panel. Calculation parameters are described in the text, the degassing pressure is set to 2 kbar.

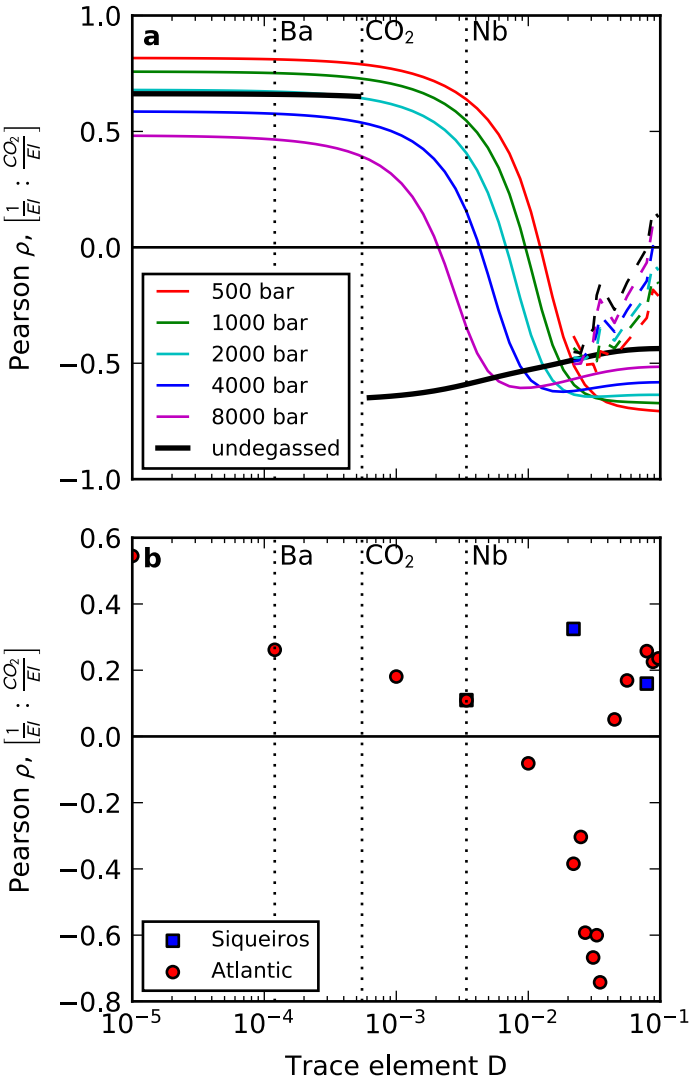

Figure 5. Panel a shows the variation of the Pearson correlation coefficient between 1/El and CO_2/El calculated for melts mixed following degassing at different pressures. A switch from positive to negative correlation is seen at increasing D as degassing pressure decreases. Since there is zero variance in CO_2/El for undegassed melts when the trace element partitions identically to CO_2, the correlation coefficient is undefined. The trace element D values are partition coefficients during mantle melting. The vertical dotted lines show the partition coefficients for Ba, CO_2 and Nb, as reported by Workman and Hart (2005) and Rosenthal et al. (2015). The dashed lines indicate the effect of garnet in the source: trace element concentrations are calculated using the alphaMELTS frontend (Smith and Asimow, 2005) for the pMELTS thermodynamic model (Ghiorso et al., 2002) using variable bulk partition coefficients calculated from constant mineral-melt partition coefficients (McKenzie and O'Nions, 1991, 1995). CO_2 concentrations were calculated by assuming identical behaviour to Ba. The calculation was run in the CFMAS-Ti system with the depleted mantle composition of Workman and Hart (2005), starting at a temperature of 1500°C at pressure of 30 kbar (sufficient for garnet to be the stable aluminous phase at the start of melting), and stopped at 2.5 kbar. The trace elements are plotted at the partition coefficients given by Workman and Hart (2005). Panel b shows the Pearson

827 correlation coefficient between CO_2/El and 1/El for the Equatorial Atlantic dataset (Le
828 Voyer et al., 2017) and the Siqueiros dataset (Saal et al., 2002).

829

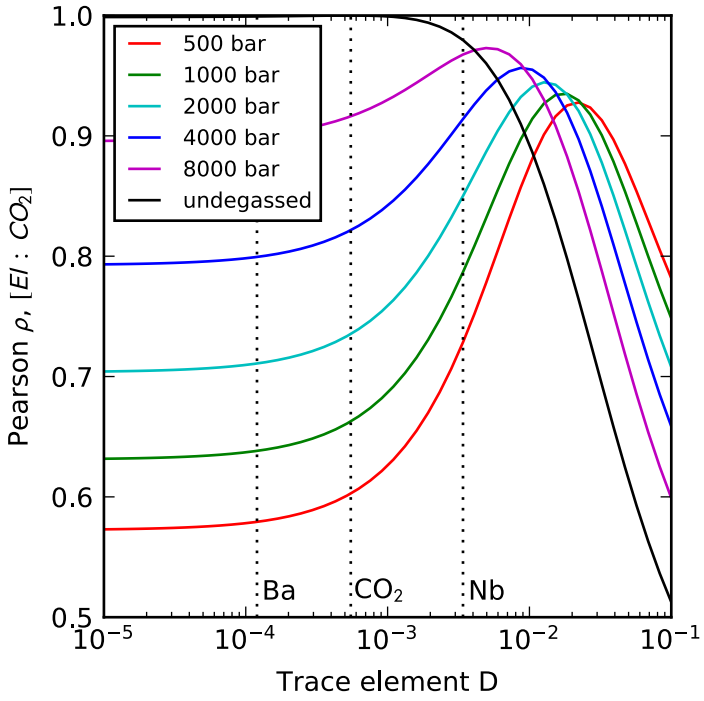

Figure 6. Variation of the Pearson correlation coefficient between concentrations of trace elements of varying partition coefficient during mantle melting (D) and CO_2 concentrations, for different pressures of degassing. When melts have partially degassed the best correlation is seen between CO2 and more compatible trace elements. See the caption to Figure 5 for description of additional lines and data sources.

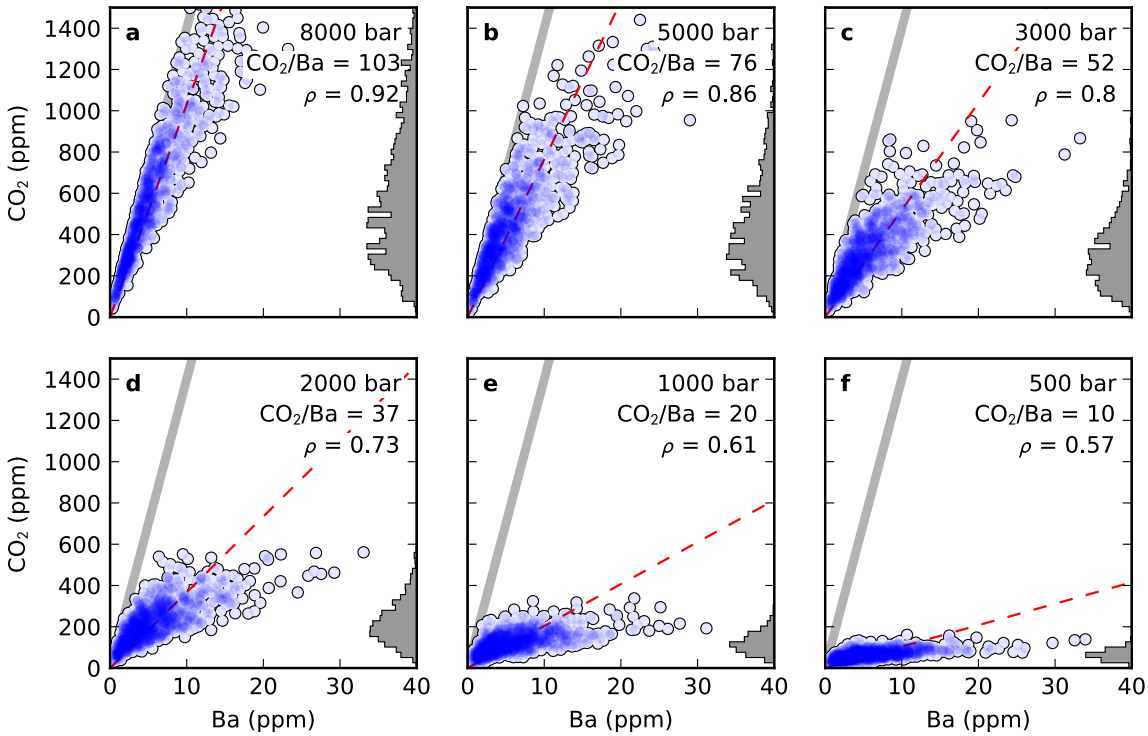

Figure 7. Each panel displays the CO2-Ba systematics generated by mixing melts degassed at different pressures (shown in bar, in the upper right corner). As the degassing pressure decreases, the array of melt compositions rotates to lower CO_2/Ba. Histograms of mixed melt density shown on the right hand side. The shading indicates density of data. The thick grey line shows the CO_2/Ba ratio of the source mantle (140), and the red-dashed line the CO_2/Ba ratio obtained by orthogonal distance regression on the mixed melts (also shown in the top right hand corner of each panel).

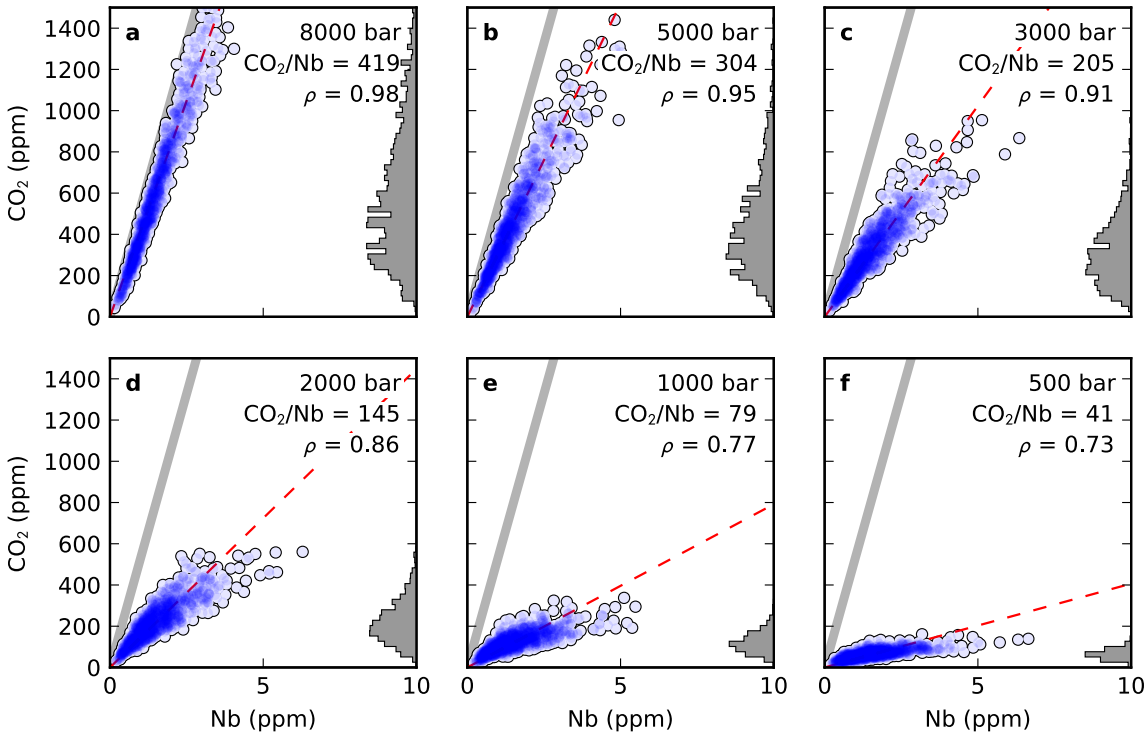

Figure 8. Each panel displays the CO_2-Nb systematics generated by mixing melts degassed at different pressures (shown in bar, in the upper right corner). As the degassing pressure decreases, the array of melt compositions rotates to lower CO_2/Nb, but with better correlations than seen for CO2 and Ba (Figure 7). Histograms of mixed melt density shown on the right-hand side. The shading indicates density of data. The thick grey line shows the CO_2/Nb ratio of the source mantle (531), and the red-dashed line the CO_2/Nb ratio obtained by orthogonal distance regression on the mixed melts (also shown in the top right hand corner of each panel). The CO_2 concentration in the mantle source is identical to that used in the calculations shown in Figure 7.

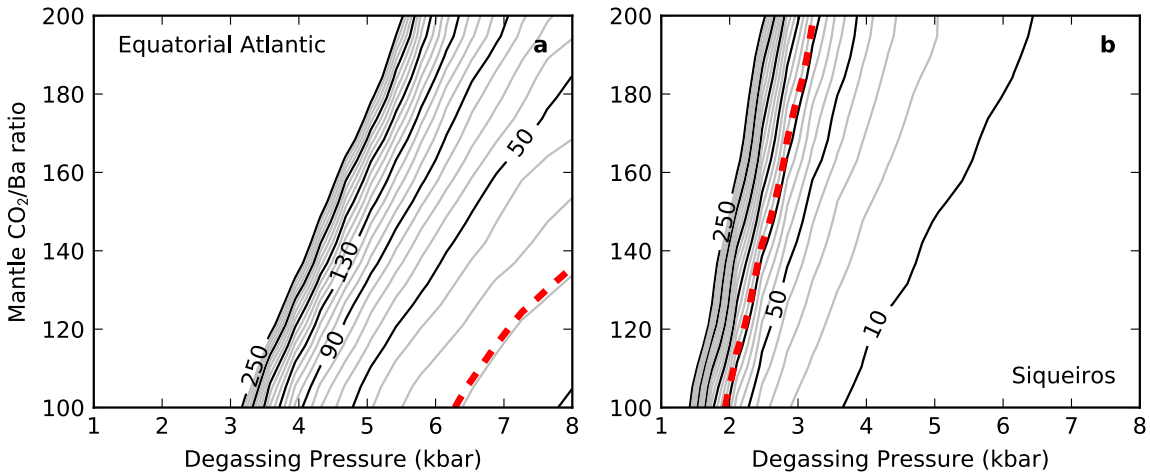

855

856 Figure 9. Contours of the minimum number of analyses required to get at least one
857 analysis (in all of 500 model runs) recording a CO_2/Ba ratio within 10% of the mantle
858 value, as a function of degassing pressure and mantle CO_2/Ba ratio. Contours are spaced
859 at intervals of 10 analyses. In panel a the melting model described in Section 2.1 is used
860 and is appropriate for the comparison to the Equatorial Atlantic dataset (Le Voyer et al.,
861 2017), which contains 21 melt inclusion analyses, indicated by the thick red dashed line.
862 Panel b uses a similar melting model, but with a mantle Ba concentration typical of the D-
863 MORB source (Workman and Hart, 2005), and is appropriate for comparison with the
864 Siqueiros dataset (Saal et al., 2002), which contains 97 analyses. In both panels the mixing
865 parameter is set to N = 16.

866

867
868 # A Effect of homogenisation during transport on CO2-trace element
869 systematics

870 Soon after mantle crosses the peridotite solidus, the melt fraction will be low and
871 the high porosity melt channels, thought to be critical in preserving primary melt
872 variability, may be yet to form. Melts may therefore homogenise at these depths,
873 Rudge et al. (2013) find such a process is required for subsequent melt mixing to produce
874 the binary isotope arrays observed in Iceland.

875 The effect of this process, with varying homogenisation depth, is shown in Figure
876 A1. As the homogenisation depth increases more melts are mixed together, and the
877 variability of the melts entering the crust is reduced. At the greatest extents of
878 homogenisation (Panels e and f), the extremely high concentrations of CO2 in the deepest
879 melts is sufficiently diluted by the addition of shallower melts that CO2 saturation is no
880 longer reached; the melts preserve the mantle CO2/Ba ratio. At more modest extents of
881 homogenisation (Panels c and d), the variability in CO2 concentration has been removed,
882 but the deepest melts are not sufficiently diluted that they do not saturate in CO2 in the
883 crust; binary mixing now takes place between a trace element enriched degassed melt,
884 and an extremely depleted undegassed melt, and the mantle CO2/Ba ratio is not
885 preserved. When only limited homogenisation takes place (Panel b), the variability of
886 melts is reduced but not sufficiently for a binary mixing array to be produced; the scatter
887 about the average ratio is considerably less than the unhomogenised case (Panel a),
888 however.

889 Since binary mixing arrays in CO2-trace element space are not observed in the
890 published datasets, it is likely that only limited homogenisation has taken place. Small
891 amounts of homogenisation do not change the results or conclusions of this paper.

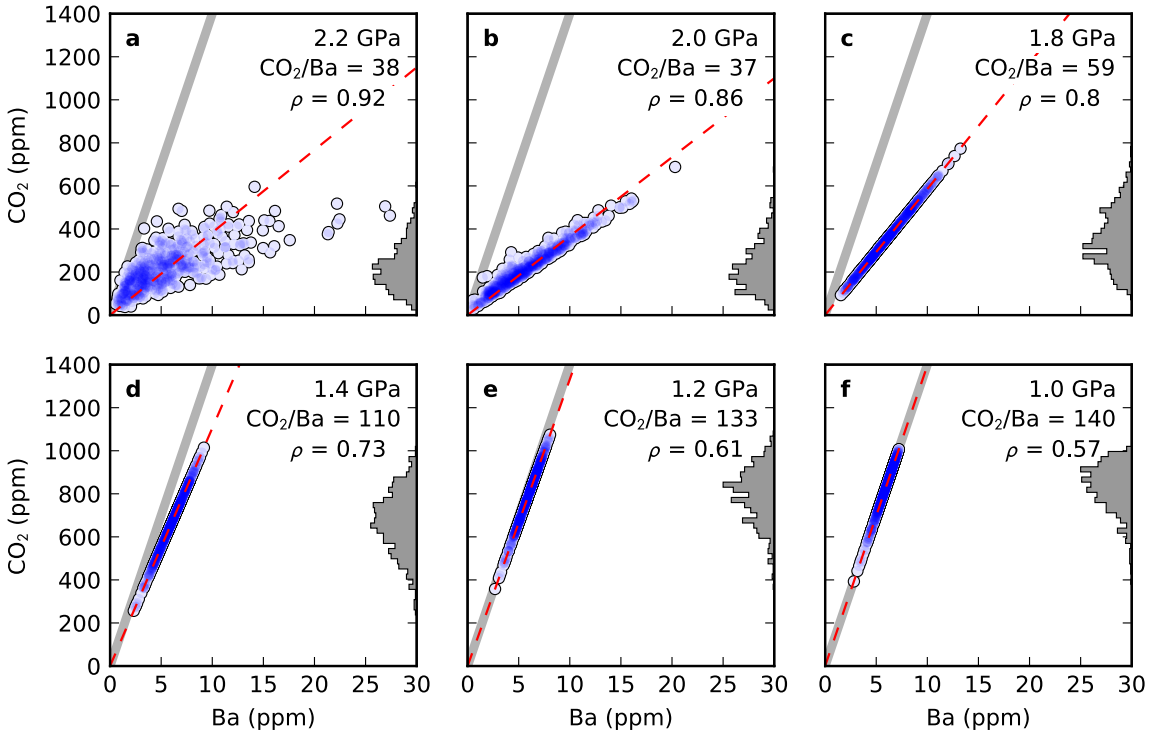

Figure A1. Each panel shows the results of the mixing-degassing calculation for melts that have been variably homogenised during transport. As the extent of homogenisation increases, the variability in the CO_2/Ba ratio decreases, and the array rotates towards the mantle CO_2/Ba ratio. The pressure in the upper-right corner of each panel shows the pressure below which all melts produced are completely mixed. Degassing occurred at 2000 bar. See Figure 7 for more information.

B Effect of Mixing parameter on CO_2-trace element systematics

The effect of the mixing parameter on the distribution of data in CO_2-trace element space in shown in Figure B1. As the mixing parameter increases, the array condenses towards the most depleted melts. A small change in the best fit ratio is seen in Figure B1, however this is due to having insufficient draws from the distribution to characterise the mean ratio accurately. As the number of analyses increases the best fit ratio will tend towards the mean ratio, regardless of mixing parameter. The smaller the degree of mixing, the more likely it is for the mantle CO_2/Ba ratio to be preserved, shown by the number of points lying on the grey line in Figure B1. The general systematics described in the main text are not affected by small changes in the mixing parameter. Estimates of the minimum number of analyses required to observe mantle CO_2/Ba ratios (Section 4.3) will be sensitive to this however, and so these results should be used with care.

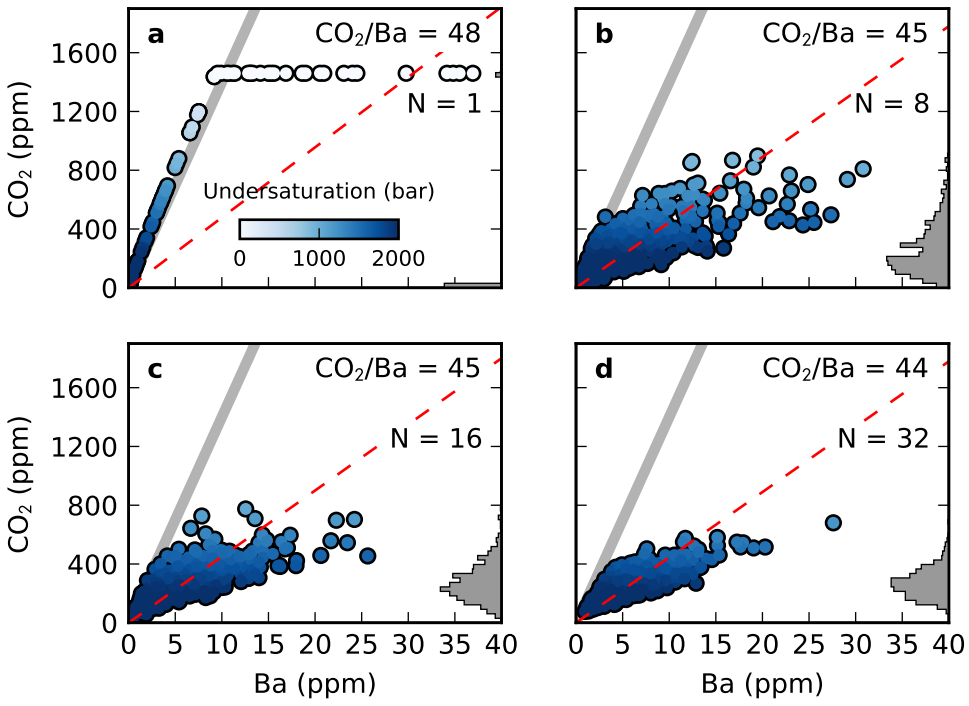

Figure B1. CO2-Ba systematics resulting from varying mixing parameter, and degassing at 2000 bar. As mixing parameter increases, the array condenses towards the depleted melt endmember. Colour indicates CO2 undersaturation at 2000 bar. See the caption to Figure 7 for further description.

917

C Sensitivity of Pearson correlation coefficient to other parameters

As described in the main text, degassing has a dramatic effect on the behaviour of the Pearson correlation coefficient between CO_2/El and 1/El, moving the change from positive to negative coefficient towards higher trace element partition coefficient. The pressure at which degassing takes place is a major control on where this transition happens, and the magnitude of the correlation coefficients either side. These properties of the correlation coefficient are not controlled uniquely by degassing pressure however, Figure C1 demonstrates how the mixing parameter, source CO2 concentration, the residual porosity during melting and homogenisation during transport (Appendix A), affects the behaviour of the correlation coefficient. Plots of this type are therefore useful for qualitatively identifying the presence of degassing, but cannot be used to extract degassing pressure quantitatively.

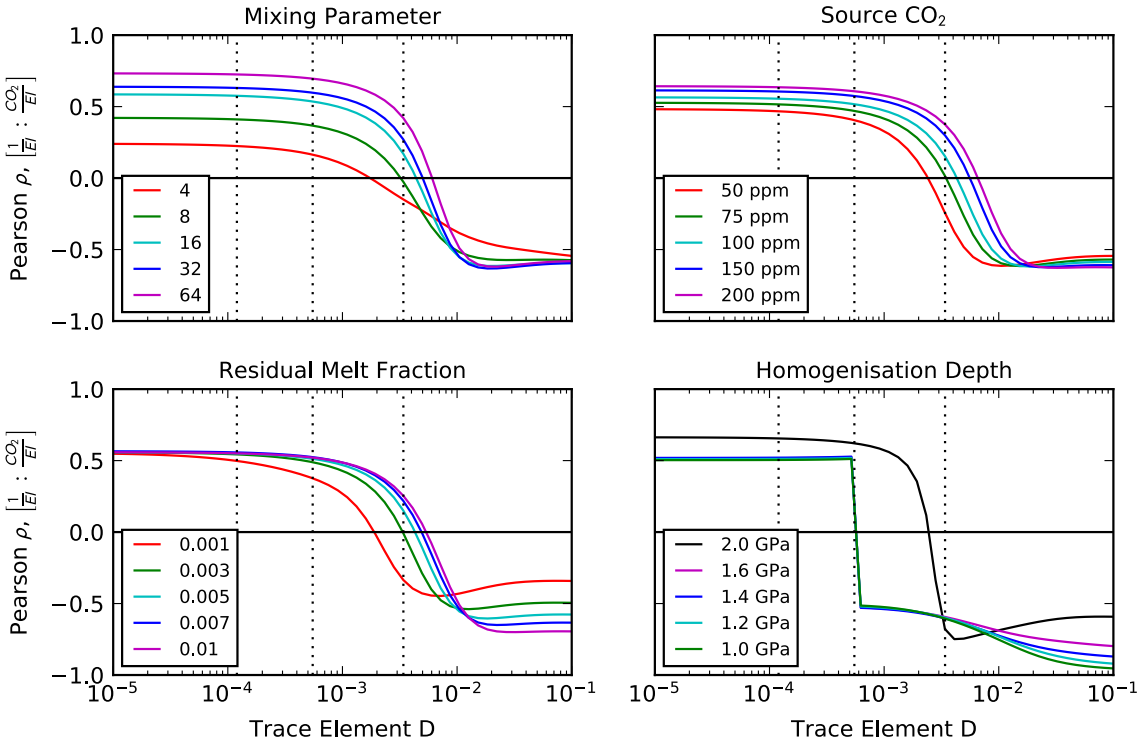

Figure C1. The effect of variables other than degassing pressure on the Pearson correlation coefficient between 1/El and CO_2/El. Calculations performed at 2000 bar, with other parameters as described in main text, unless noted in the panel key.